

Identification of a BAZ2A-Bromodomain Hit Compound by Fragment Growing

Andrea Dalle Vedove, Giulia Cazzanelli, Laurent Batiste, Jean-Rémy Marchand, Dimitrios Spiliotopoulos, Jessica Corsi, Vito Giuseppe D'Agostino, Amedeo Caflich,* and Graziano Lolli*



Cite This: *ACS Med. Chem. Lett.* 2022, 13, 1434–1443



Read Online

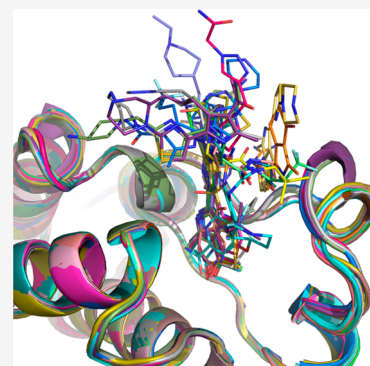
ACCESS |

Metrics & More

Article Recommendations

Supporting Information

ABSTRACT: BAZ2A is an epigenetic regulator affecting transcription of ribosomal RNA. It is overexpressed in aggressive and recurrent prostate cancer, promoting cellular migration. Its bromodomain is characterized by a shallow and difficult-to-drug pocket. Here, we describe a structure-based fragment-growing campaign for the identification of ligands of the BAZ2A bromodomain. By combining docking, competition binding assays, and protein crystallography, we have extensively explored the interactions of the ligands with the rim of the binding pocket, and in particular ionic interactions with the side chain of Glu1820, which is unique to BAZ2A. We present 23 high-resolution crystal structures of the holo BAZ2A bromodomain and analyze common bromodomain/ligand motifs and favorable intraligand interactions. Binding of some of the compounds is enantiospecific, with affinity in the low micromolar range. The most potent ligand has an equilibrium dissociation constant of 7 μ M and a good selectivity over the paralog BAZ2B bromodomain.



KEYWORDS: BAZ2A bromodomain, Prostate cancer, Fragment growing, X-ray crystallography, Molecular docking, Binding assays

Bromodomains are epigenetic readers of acetylated lysines (Kac) in histones and other proteins. The human genome comprises 61 bromodomains in 46 proteins that also include additional DNA or protein-recognition/modifying domains (acetylases, PHD zinc fingers, helicases, and methyltransferases).¹ Due to their involvement in the regulatory machinery of chromatin conformation and accessibility, bromodomains have been recognized as promising drug targets, especially in cancer and inflammatory diseases. Various small-molecule inhibitors have been developed, with some of them in clinical trials.²

BAZ2A (bromodomain adjacent to zinc finger domain protein 2A) is one of the nucleolar remodeling complexes mediating chromatin condensation and silencing of ribosomal DNA (rDNA).^{3,4} However, its role extends beyond the epigenetic modulation of rDNA transcription. In prostate cancer, BAZ2A is overexpressed and cooperates with EZH2 (enhancer of zeste homolog 2) in potentiating tumor cells' migration and metastatic potential.^{5,6} BAZ2A has then been proposed as a prognostic marker for aggressive and recurrent prostate cancer as well as a promising therapeutic target. BAZ2A inhibition has been found to synergize with BET (bromodomain and extra-terminal domain) inhibitors in suppressing growth in TNBC (triple-negative breast cancer) cells.⁷ Very effective anti-proliferative activity was obtained by simultaneous inhibition of the BET bromodomains and the non-BET members BRD9 and BAZ2A.

BAZ2A, however, features a shallow pocket, making it one of the least druggable bromodomains.⁸ Only two chemical probes

have been developed so far, namely GSK2801 and BAZ2-ICR, with affinities in the very high nanomolar range.^{9,10} A rationale for improving BAZ2A inhibitors is to look for additional interactions with residues located at the tip of its binding pocket.¹¹

Here we present the optimization of a series of ligands of the BAZ2A bromodomain by structure-based fragment growing.

An initial set of about 50 000 molecules was selected in parallel using two different computational methods: a protein-based search and a ligand-based procedure. The first method consisted of a Pharmit search¹² starting from a parent fragment identified in a previous screening campaign (compound 1 in ref 11) for the pharmacophoric definition. The ligand-based procedure consisted of a selection of the ZINC15 library¹³ limited to molecules with up to three rotatable bonds. In both cases, only compounds bearing a positive charge were kept, with the aim of reaching BAZ2A Glu1820 at the rim of the pocket as a putative determinant for increased potency and selectivity (Figure S1, structural alignment of representative bromodomains). The resulting 50 000 molecules were screened by automatic docking (see the Supporting

Received: April 12, 2022

Accepted: June 22, 2022

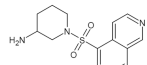
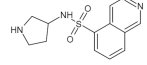
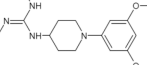
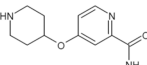
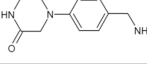
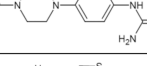
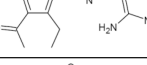
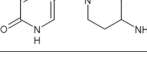
Published: August 3, 2022



Information for details). The docked poses were ranked by a force-field-based energy function with approximation of desolvation effects in the continuum-dielectric representation.^{14,15} A total of 80 molecules were selected, for which commercial availability was checked, and 36 were obtained (Table S1).

The 36 selected molecules were tested by AlphaScreen at single doses in duplicate. Six molecules (compounds 8, 9, 11, 14, 18, and 25) decreased binding of BAZ2A bromodomain to the acetylated peptide by at least 50% when tested at 500 μ M. The IC₅₀ was evaluated for those compounds, resulting in binding inhibition in the high micromolar range, except for compound 25, which performed significantly better than the others (Figure S2 and Table 1).

Table 1. BAZ2A Binding Fragments Identified by Docking and Validated by Competitive Binding Assay or X-ray Crystallography

CMP	Structure	% residual BAZ2A activity ^a	IC ₅₀ BAZ2A (μ M)
8		49 \pm 7	> 200
9		44 \pm 3	> 200
11		48 \pm 5	> 200
13		75 \pm 2	n.d.
14		32 \pm 4	> 200
18		37 \pm 4	> 200
25		5 \pm 0.6	33.2 \pm 0.3 (R ² = 0.89)
36		71 \pm 3	n.d.

^aThe single-dose experiment was carried out at a compound concentration of 500 μ M.

All 36 fragments were also screened in co-crystallization experiments with the BAZ2A bromodomain. For about half of the compounds, crystals did not grow or only diffracted to very poor resolution, including the active fragments 8, 11, and 14, suggesting an interference with the crystallization process. Various BAZ2A apo crystals were obtained in co-crystallization with compounds showing <20% inhibition at 500 μ M, confirming they are not BAZ2A binders. Co-crystals were obtained with fragments 9, 13, 18, 25, and 36.

All compounds bind in the Kac pocket with their respective headgroups sandwiched between Val1822 and Val1879, anchoring through a hydrogen bond to side chains of Asn1873 or Tyr1830 (via the conserved W1 water molecule) or both (Figure 1a).

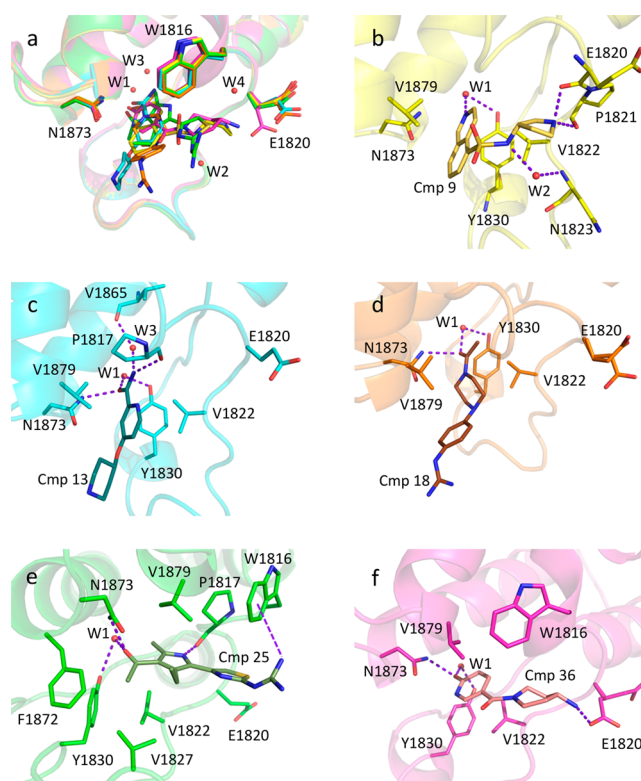


Figure 1. Binding mode of fragments to the BAZ2A bromodomain. (a) Headgroups of the different fragments are involved in similar contacts with the protein matrix. (b–f) Binding poses of compounds 9 (b), 13 (c), 18 (d), 25 (e), and 36 (f).

In compound 9, the only direct H-bonds with the protein matrix are between the pyrrolidine nitrogen and both Glu1820 and Pro1821 main-chain oxygens, while the interactions of the isoquinoline nitrogen with Tyr1830 and of the sulfonamide nitrogen with Asn1823 main-chain nitrogen are mediated by W1 and W2 (Figure 1b). Despite the limited resolution, the electron density supports the largely preferential, if not exclusive, binding to BAZ2A of the single *S* enantiomer.

The binding mode of compound 13 is unexpected (Figure 1c). It runs parallel to the end of the α B helix, similarly to the Kac residue of acetylated peptides, instead of facing the WPF shelf of the ZA loop. Consequently, the charged piperidine is not directed toward Glu1820 but rather exposed to the solvent. The amide of compound 13 does not reciprocally interact with the side chain of Asn1823, unusually placing the amide nitrogen in the small pocket reserved for the KAc methyl group in physiological ligands. While the amide oxygen interacts with both Asn1823 and Tyr1830 (W1-bridged), the amide nitrogen establishes H-bonds to main-chain oxygens of Pro1817 and Val1865, the latter mediated by a water molecule (W3).

Compound 18 binds with a similar orientation with respect to 13 (Figure 1d). The 18 acetyl group, almost superposed to the 13 amide, again contacts Asn1823 and Tyr1830 through its oxygen, while the methyl group is correctly positioned in the corresponding hydrophobic pocket. The charged guanidinium is exposed to the solvent far away from Glu1820.

In compound 25, the acetyl-pyrrole headgroup shows extended interactions with the protein matrix (Figure 1e). The pyrrole nitrogen is in H-bond contact with the Pro1817 main-chain oxygen. The methyl group in position 2 nicely fits the corresponding KAc methyl cavity. The 3-acetyl substituent

Table 2. Activity of Conjugated Acetylpyrrole-Thiazole Compounds as BAZ2A Binders

CMP	Structure	IC50 BAZ2A (μM)	CMP	Structure	IC50 BAZ2A (μM)
43		76.2 \pm 8.6 ($R^2 = 0.61$)	57		93.2 \pm 10.1 ($R^2 = 0.60$)
44		57.9 \pm 6.0 ($R^2 = 0.79$)	58		> 100
45		109.2 \pm 12.3 ($R^2 = 0.73$)	59		74.2 \pm 9.1 ($R^2 = 0.61$)
47		33.3 \pm 0.4 ($R^2 = 0.91$)	60		> 100
48		94.6 \pm 11.7 ($R^2 = 0.71$)	61		54.0 \pm 0.2 ($R^2 = 0.91$)
49		47.0 \pm 5.0 ($R^2 = 0.80$)	62		53.9 \pm 0.2 ($R^2 = 0.89$)
50		76.8 \pm 6.4 ($R^2 = 0.72$)	63		60.5 \pm 9.4 ($R^2 = 0.67$)
52		93.5 \pm 9.7 ($R^2 = 0.67$)	64		75.7 \pm 9.2 ($R^2 = 0.61$)
53		54.0 \pm 0.2 ($R^2 = 0.93$)	65		54.0 \pm 0.3 ($R^2 = 0.84$)
54		61.3 \pm 10.6 ($R^2 = 0.62$)	66		99.7 \pm 10.9 ($R^2 = 0.78$)
55		114.0 \pm 22.1 ($R^2 = 0.55$)	69		74.3 \pm 4.7 ($R^2 = 0.76$)
56		> 100	72		54.6 \pm 7.1 ($R^2 = 0.75$)

forms the usual H-bonds with Asn1873 and Tyr1830, while the methyl group is in hydrophobic contact with Val1827, Tyr1830, and Phe1872. The ethyl group in position 4 contributes through hydrophobic and van der Waals interactions with Val1822, Val1827, and Val1879. The thiazole-guanidine moiety is rotated by about 180° with respect to the expected pose. While the thiazole ring is in π -stacking interaction (T-shaped) with Trp1816 as expected, the guanidinium group is not directed toward Glu1820 but instead forms a π -cation interaction again with Trp1816, although with sub-optimal geometry.¹⁶ The above-reported interactions support the relevant binding affinity observed for compound 25.

The pyridone oxygen of compound 36 consistently interacts with Asn1823 and Tyr1830 (Figure 1f). The amino-piperidine

tail is in hydrophobic and van der Waals contact with Trp1816; its charged, terminal nitrogen finally contacts the Glu1820 side chain. Electron density indicates that, together with the predominant *pt* conformer ($\chi_1 = 63^\circ$) forming the ionic interaction with compound 36, Glu1820 also assumes the *mm* rotameric form ($\chi_1 = -65^\circ$), exposing its carboxylate to the solvent. This suggests that contribution to the binding energy of the salt bridge with Glu1820 is limited, at least for this compound, while potentially relevant for selectivity against other bromodomains.

We then set out to optimize fragment 25. A sub-structure search on the ZINC15 database of commercially available compounds was conducted using the 3-acetyl-2,4-dimethyl-5-thiazole-pyrrole structure as a query. Compounds 37–73 (Table S2), all bearing a substituent in position 2 of the

thiazole ring, were selected and their activities tested on the BAZ2A bromodomain by Alphascreen in single doses of 500 μ M (Figure S3).

Compounds 37–41, all bearing an aromatic 6-membered ring conjugated to the thiazole ring, were poorly active. Compounds substituted with aromatic 5-membered rings displayed some activity, although not evenly (e.g., 69 vs 68). Nonplanar 5- or 6-atom heterocycles are generally well accepted, either directly linked to the thiazole ring or with a bridging methyl group, as well as linear groups. Generally, positively charged substituents performed better than polar groups (e.g., 49 vs 51), while hydrophobic derivatives were ineffective (e.g., compound 42).

Compounds showing inhibition of the BAZ2A bromodomain binding to the acetylated peptide by at least 67% in single doses were further tested for dose–response, together with the minimal compound 43 as reference. This screen identified that compound 47 was as active as 25 (Table 2 and Figure S4). Binding affinity is influenced by the number and location of nitrogen atoms in the tail groups. This can be deduced when comparing compounds 47 (holding a piperazine ring) and 48–50 (4-, 3-, and 2-piperidine). The favorable contribution deriving from a positive charge is again evident when comparing 53 and 54 with 55–58 (charged vs uncharged pyrrolidine rings).

We determined the crystallographic structures for six compounds in complex with BAZ2A, namely 44, 45, 47, 61, 63, and 65. The most striking difference between these compounds and 25 is the 180° rotation of the thiazole ring with the subsequent different orientations assumed by the tails departing from it (Figure 2a).

The 3-aminopropyl substituent in compound 44 performs better than the *N*-methyl-2-aminoethyl group of 45. Binding poses of compounds 44 and 45 are similar: all interactions of the acetyl-pyrrole headgroup are conserved with respect to 25, but the charged tails do not point toward Trp1816, but instead approach Glu1820 (Figure 2b,c). However, as observed in compound 36, Glu1820 oscillates between two conformers, one in contact with the compound amino group and the other exposed to the solvent; this interaction seems to contribute only partially to the binding affinity. Instead, compound 44 is involved in a network of water-mediated interactions with the protein matrix (Figure 2b). The thiazole nitrogen forms a hydrogen bond with water W4, which tetrahedrally interacts with the main chain of Pro1817 and water molecules W5 and W6, in turn in contact with BAZ2A. Water W5 is tetrahedrally coordinated by the terminal amino group of 44, the Trp1816 main-chain oxygen, the Leu1819 main-chain nitrogen, and W4. The interaction between the secondary amine and W5 is missing in compound 45, justifying its lower affinity when compared to 44 (Figure 2c). Despite the observed interaction patterns, both compounds have poor affinity for BAZ2A, most probably due to the entropic penalty deriving from the freezing of the alkylamine tails and the surrounding water network.

Compound 47 binds similarly to 44 and 45. Better affinity derives from increased rigidity and bulkiness, resulting in additional van der Waals contacts with Trp1816 (Figure 2d). Similarly, the extra rigidity of the 47 piperazine with respect to the piperidine rings of compounds 48–50, where the thiazole-linked planar nitrogen is substituted with a tetrahedral carbon, may explain the observed preference for the piperazine ring. Notably, in the structures in complex with 44, 45, and 47, an ethylene glycol molecule is sandwiched between the thiazole

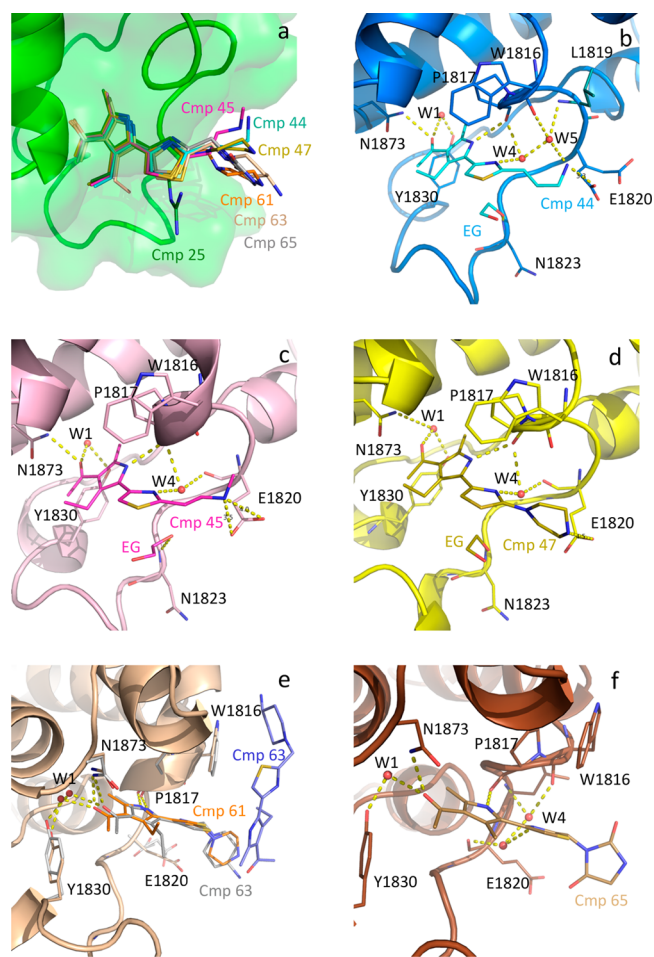


Figure 2. Binding mode of acetylpyrroles to the BAZ2A bromodomain. (a) Compounds are almost identically placed in their headgroup region but differ in the orientation of their tail moieties. (b–f) Binding poses and interactions for compounds 44 (b), 45 (c), 47 (d), 61 (e), 63 (f), and 65 (g). In panels b–d, the ethylene glycol molecule is indicated with EG. In panel e, compound 61 is in orange, the two copies of compound 63 are in gray and violet, and relevant amino acids are in wheat (in the complex with 61) and white (in the complex with 63).

ring and the ZA loop (Figure 2b–d). It forms a hydrogen bond with the main-chain nitrogen of Asn1823, an important anchoring point already explored by the BAZ-ICR and GSK2801 chemical probes and other BAZ2A inhibitors,^{9,10,14} and a relevant indication for further optimization of this chemical class.

Slightly more protruding tails are present in compounds 59–65 (Figure 2a). Compounds 59, 61–64, and, more unexpectedly, compound 65 (imidazolidinedione tail) retained a good activity although lower than compound 47. The 61 piperazine ring faces Glu1820 at a distance of 4 Å (Figure 2e). The more protruding amino-terminal of compound 63 interacts with Asp1798 of a symmetry-related chain. Given the very similar activity of the two compounds, it is reasonable to suppose that Asp1798 from the symmetric mate artifactually competes in the crystal with Glu1820 for the binding to 63. Again, and in both cases, the contribution to the binding energy of the ionic interaction with Glu1820 appears limited. Interestingly, an additional copy of compound 63 is present at the interface between symmetry-related protein chains, with its 1-(2-thiazolylmethyl)-4-piperidinamine moiety stacking almost

Table 3. Compounds Screened in the Fragment-Growing Campaign^a

CMP	Structure	IC50 BAZ2A (μM)	CMP	Structure	IC50 BAZ2A (μM)
74		> 100	95		12.9 ± 2.0 (R ² = 0.95)
75		n.d.*	96		85.1 ± 6.8 (R ² = 0.69)
76		n.d.*	97		49.3 ± 5.7 (R ² = 0.77)
77		38.9 ± 2.0 (R ² = 0.91)	98		12.6 ± 1.4 (R ² = 0.71)
78		40.1 ± 3.4 (R ² = 0.85)	99		10.9 ± 0.2 (R ² = 0.94)
79		12.5 ± 0.4 (R ² = 0.89)	100		36.5 ± 4.1 (R ² = 0.90)
80		11.4 ± 0.3 (R ² = 0.94)	101		n.d.*
81		11.8 ± 0.3 (R ² = 0.88)	102		10.6 ± 0.2 (R ² = 0.98)
82		44.6 ± 5.6 (R ² = 0.74)	103		n.d.*
83		11.0 ± 0.2 (R ² = 0.91)	104		4.0 ± 0.2 (R ² = 0.96)
84		29.2 ± 0.3 (R ² = 0.88)	105		33.2 ± 0.3 (R ² = 0.93)
85		n.d. [#]	106		n.d.*
86		> 100	107		14.1 ± 0.2 (R ² = 0.92)

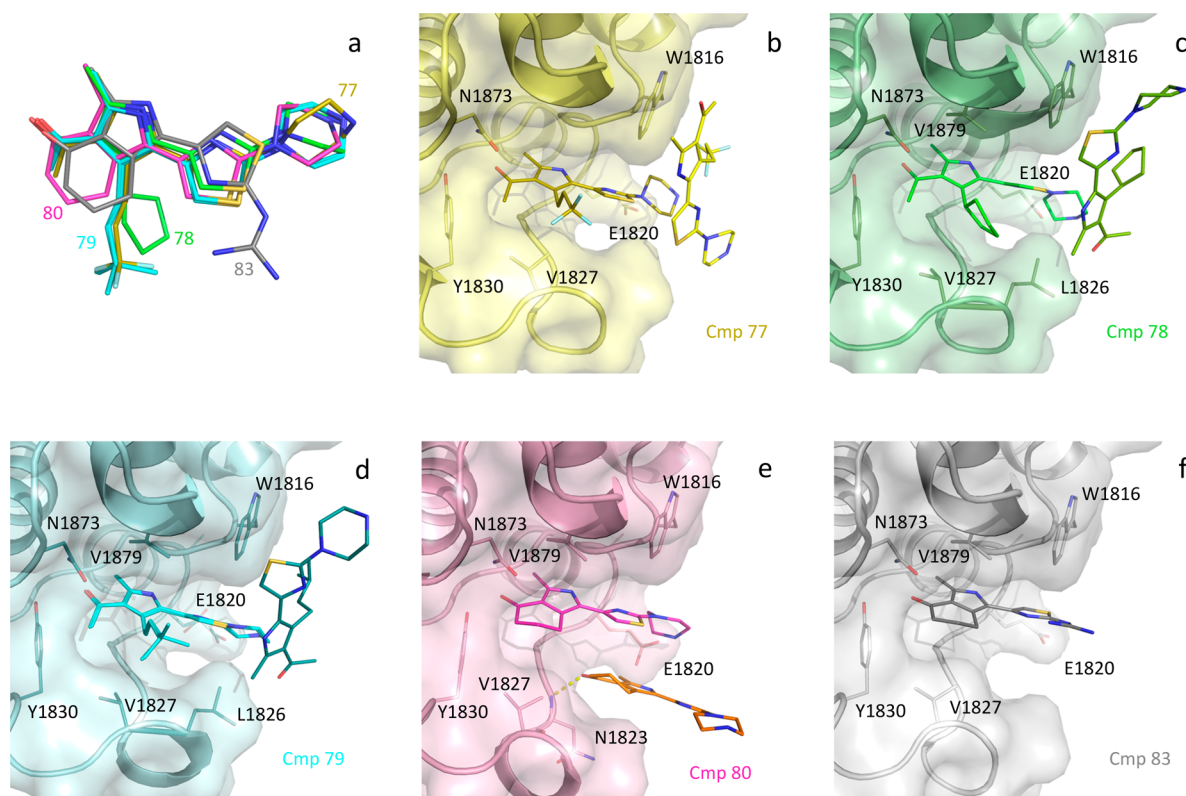


Figure 3. Binding poses of compounds 77–80 and 83 (a). A second copy of the inhibitor is present, stacking either to W1816 (compounds 77, 78, and 79, panels b, c, and d, respectively) or to itself and hydrogen bonding to N1823 main-chain nitrogen (80, panel e). The tail of compound 83 is oriented differently with respect to the other compounds (panels a and f).

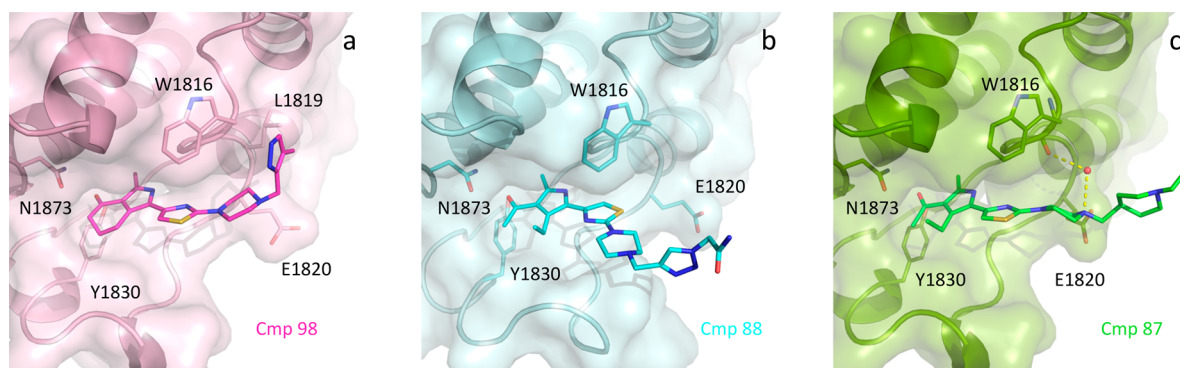


Figure 4. Binding poses of compounds 98, 88, and 87. The tail of 98 is in contact with Trp1816 and Leu 1819 (a), while in compounds 88 and 87 (b, c) the tails are exposed to the solvent with minimal contacts with the protein matrix.

Leu1826 and Val1827 are formed by the bulkier substituents of compounds 78–79 (Figure 3c,d). However, the cyclopentyl group in compound 78 is squeezed between the two above residues, Val1879 and the thiazole ring, with excessive crowding in this region. This is confirmed in compounds 80–84, where the gain obtained in 80 and 83 through cyclization of the headgroup is not reinforced by the extra methyl groups in 81, 82, and 84. Comparison of binding poses for compounds 80 and 83 confirms the different orientations of the piperazine and guanidinium tails (Figure 3a,e,f), as observed for 25 and 47 (Figure 2a).

For compounds 86–99, tails in position 4 of the piperazine ring were designed to stack with Trp1816 via π – π or cation– π interactions. None of them resulted in improved affinity with respect to compound 47 (Figure S5), suggesting that stacking

interaction with the solvent-exposed Trp1816 does not significantly contribute to the binding energy. Indeed, in the BAZ2A-compound 98 co-crystal structure, the methyl-pyrazole tail contacts Trp1816 and Leu1819 as expected, but no significant improvement in affinity is appreciable (Figure 4a). Surprisingly, compound 88, bearing a similar acetamide-triazole tail, assumes a different pose, with the thiazole ring rotated by 180° (as observed in 25) and the subsequent acetamide-triazole tail fully solvent-exposed (Figure 4b). Similarly, the IC_{50} value for compound 87 is not lower than that for 47; here, the piperazine ring is located as in the parent molecule 47 with its N4 atom at 3.9 Å from Glu1820 and also in hydrogen-bond contact with a water molecule bridging the inhibitor to Trp1816 carbonyl oxygen (Figure 4c). However, the extra ethyl-piperidinyl group protrudes linearly from the

pocket and is exposed to the solvent without additional interaction with the protein matrix.

Derivatization in position 2 of the piperazine ring was more successful, yielding six compounds with improved affinity and, among these, compound **104** with an 8-fold increase in potency with respect to **47** (Table 3 and Figure S5). Notably, the piperazine C2 is a stereocenter in this class of compounds, and all of them were tested as racemic mixtures. We determined the crystallographic structures for compounds **104**, **109**, **111**, and **113**; in all of them, the thiazole ring reverses to the orientation observed in compound **25**, and only the R enantiomer binds in the BAZ2A pocket. Compounds **111** and **113** bear a hydrophobic tail, providing additional contacts with Leu1826 and Val1827 (Figure 5a). An ethylene glycol molecule, located as in the structures with compounds **44**, **45**, and **47**, also connects the amide nitrogen of **111** to the main-chain nitrogen of Asn1823. Compound **109** establishes the same H-bond with Asn1823 main chain through its

terminal hydroxyl group (Figure 5b); however, an entropic penalty is conceivable considering the significant flexibility of the *n*-butanol tail. The higher affinity of **104** is evident: the ethyl-isoxazole tail turns back into the pocket, with its aromatic ring stacking almost parallel to the thiazole ring and establishing van der Waals interactions with Leu1826 and Val1827 and the hydrogen bond with Asn1823 main-chain nitrogen (Figure 5b). The important contribution of this H-bond to BAZ2A inhibitors has already been reported in both BAZ2 chemical probes GSK2801 and BAZ2-ICR and in a triazole-based BAZ2A hit compound. These last two also reproduce the four-layer sandwich observed in **104**, with the two aromatic rings squeezed between Trp1816 and Leu1826 (Figure 5c).^{9,10,17} The decreased ligand efficiency (LE) of **104** compared to the parent compounds **25** and **47** (0.24 vs 0.31 and 0.29 kcal/mol per heavy atom, respectively) is compensated however by a more favorable lipophilic ligand efficiency (LLE, 4.0 vs 2.4 and 1.9, respectively).

The thermodynamic parameters for compound **104** binding to the BAZ2A bromodomain were finally characterized by isothermal titration calorimetry (ITC). ITC confirmed the observed enantioselectivity showing that the active fraction is about half of the racemic mixture (Figure 5d). The equilibrium dissociation constant (K_D) of 7.1 μ M is in good agreement with the IC_{50} of 4.0 μ M measured by AlphaScreen. The presence of 0.25% DMSO in the ITC experiment leads to a slightly less favorable K_D value as DMSO competes for binding to the conserved Asn.^{18,19} Binding is dominated by a relevant enthalpic contribution partially counteracted by an entropic penalty in accordance with the various interactions observed in the crystal structure combined with the freezing of the ethyl-isoxazole tail. Finally, **104** shows good selectivity over the closely related BAZ2B bromodomain, and the highest achieved so far, with an IC_{50} of 33.5 μ M, as determined by AlphaScreen (Figure S6). As compared with previous screening campaigns,^{8,11,17} such selectivity was obtained in the context of a reasonable LE and optimal log *P*, log *D*, and LLE.

The acetylpyrrole headgroup has already been explored in BRD4 and CREBBP inhibitors (Figure 5e,f), also cross-reacting with BRD7, BRD9, and HDACs.^{20–22} However, compound **104** features a unique thiazole ring as scaffold. Furthermore, its binding mode is different, as its ethyl-isoxazole tail folds back in the bromodomain Kac pocket and stacks with the thiazole ring.

The extensive chemical space exploration for the derivatization of the acetylpyrrole-thiazole scaffold toward a BAZ2A hit compound allows drawing various conclusions.

First, the pay-off for the inhibitors' extension toward the binding pocket rim or outside it in the region of Trp1816 or Glu1820 is limited, at least in terms of potency. Nonetheless, positively charged groups are better accepted and provide selectivity over the paralog BAZ2B bromodomain. A more significant gain in potency can be instead obtained moving toward the more hydrophobic region of the pocket rim in the area of Leu1826, Val1827, and Phe1872. The best reward is finally obtained by saturating the pocket, with a substantial profit deriving from both additional interactions with the protein matrix (i.e., Asn1823) and intramolecular aromatic stacking in the inhibitor, generating the four-layer sandwich with Trp1816 and Leu1826.

As observed for other bromodomains,^{23–28} the BAZ2A pocket can be targeted enantiospecifically. This, other than providing a selectivity determinant, also offers excellent

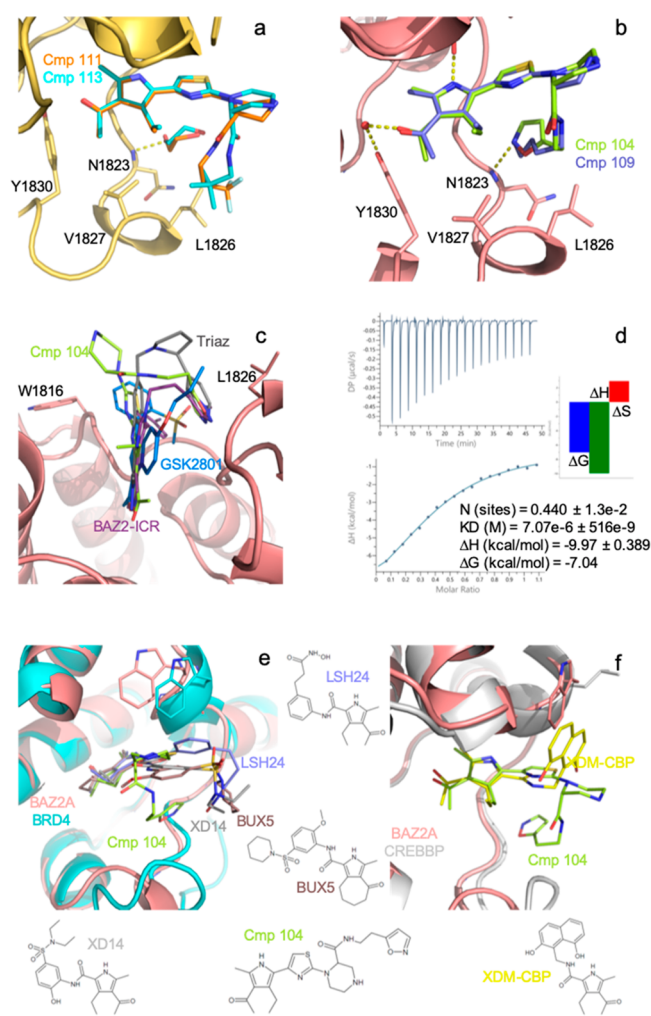


Figure 5. (a) Tails of compounds **111** and **113** provide additional contacts with Leu1826 and Val1827. (b) Compounds **104** and **109** form a hydrogen bond with the Asn1823 main chain. (c) An intramolecular stacking is observed in **104**, as similarly obtained with BAZ2-ICR (PDB 7BL8) and the triazole compound **21** of ref 16. (d) ITC titration for compound **104** showing an enthalpically driven binding restricted to a single enantiomer. (e, f) Compound **104**'s tail is oriented differently with respect to those of previously developed acetylpyrrole inhibitors directed against BRD4 (e) and CREBBP (f).

negative controls for further characterization of the BAZ2A mechanism of action. In conclusion, the hit compound **104** has an IC_{50} of 4 μ M (AlphaScreen) and a K_D of 7 μ M (ITC). The enthalpic contribution to the binding free energy of compound **104** is nearly -10 kcal/mol, which originates from its favorable interactions with the bromodomain and the stacking of its isoxazole and thiazole rings. Furthermore, we have disclosed a set of 23 holo crystal structures and related binding affinity values for compounds that bear a positively charged functional group. These data can be used to benchmark docking algorithms and scoring functions for the correct treatment of ionic groups partially or fully exposed to solvent (Supporting Information).

■ ASSOCIATED CONTENT

SI Supporting Information

The Supporting Information is available free of charge at <https://pubs.acs.org/doi/10.1021/acsmmedchemlett.2c00173>.

Tables S1 and S2, 2D structures of compounds **1–73**; Tables S3–S6, X-ray data collection and refinement statistics for all determined crystallographic structures; Figure S1, structural alignment; Figures S2–S6, AlphaScreen single-dose tests and dose–response curves for selected compounds; and Figure S7, $F_o - F_c$ electron density maps for compounds whose structure in complex with the BAZ2A bromodomain are described herein (PDF)

Accession Codes

BAZ2A structures were deposited to the PDB with accession numbers 7QZT (9), 7QVT (13), 7R01 (18), 7QVU (25), 7QVV (36), 7QWU (44), 7QWF (45), 7R0B (47), 7QWY (61), 7QX2 (63), 7QX9 (65), 7QXL (77), 7QYE (78), 7QYO (79), 7QYT (80), 7QZ0 (83), 7QZ4 (87), 7QYU (88), 7QZB (98), 7QZC (104), 7QYV (109), 7QYW (111), and 7QZI (113). Atomic coordinates and experimental data will be released upon article publication.

■ AUTHOR INFORMATION

Corresponding Authors

Amedeo Caffisch – Department of Biochemistry, University of Zürich, CH-8057 Zürich, Switzerland; orcid.org/0000-0002-2317-6792; Email: caffisch@bioc.uzh.ch

Graziano Lolli – Department of Cellular, Computational and Integrative Biology - CIBIO, University of Trento, 38123 Povo - Trento, Italy; orcid.org/0000-0002-8536-5599; Email: graziano.lolli@unitn.it

Authors

Andrea Dalle Vedove – Department of Cellular, Computational and Integrative Biology - CIBIO, University of Trento, 38123 Povo - Trento, Italy

Giulia Cazzanelli – Department of Cellular, Computational and Integrative Biology - CIBIO, University of Trento, 38123 Povo - Trento, Italy

Laurent Batiste – Department of Biochemistry, University of Zürich, CH-8057 Zürich, Switzerland

Jean-Rémy Marchand – Department of Biochemistry, University of Zürich, CH-8057 Zürich, Switzerland; orcid.org/0000-0002-8002-9457

Dimitrios Spiliotopoulos – Department of Biochemistry, University of Zürich, CH-8057 Zürich, Switzerland; Present

Address: Xenometrix AG, Gewerbestr. 25, CH-4123, Allschwil, Switzerland

Jessica Corsi – Department of Cellular, Computational and Integrative Biology - CIBIO, University of Trento, 38123 Povo - Trento, Italy

Vito Giuseppe D'Agostino – Department of Cellular, Computational and Integrative Biology - CIBIO, University of Trento, 38123 Povo - Trento, Italy

Complete contact information is available at:

<https://pubs.acs.org/doi/10.1021/acsmmedchemlett.2c00173>

Notes

The authors declare no competing financial interest.

■ ACKNOWLEDGMENTS

We are grateful to the staff of XRD1 and XDR2 beamlines, Elettra Synchrotron Light Source (Trieste, Italy), and of ID30-A1 beamline, European Synchrotron Research Facility (Grenoble, France), for on-site and remote assistance. Figures were prepared with PyMOL. The research leading to these results has received funding from AIRC under MFAG 2017 - ID. 19882 project – P.I. Lolli Graziano. A.C. is a recipient of an Excellence Grant [310030B-189363] from the Swiss National Science Foundation.

■ ABBREVIATIONS

BAZ2A, bromodomain adjacent to zinc finger domain protein 2A; BET, bromodomain and extra-terminal domain; EZH2, enhancer of zeste homolog 2; Kac, acetylated lysine; NoRC, nucleolar remodeling complex; TNBC, triple-negative breast cancer

■ REFERENCES

- (1) Filippakopoulos, P.; Knapp, S. Targeting bromodomains: epigenetic readers of lysine acetylation. *Nat. Rev. Drug Discovery* **2014**, *13*, 337–356.
- (2) Cochran, A. G.; Conery, A. R.; Sims, R. J., 3rd. Bromodomains: a new target class for drug development. *Nat. Rev. Drug Discovery* **2019**, *18*, 609–628.
- (3) Strohner, R.; Nemeth, A.; Jansa, P.; Hofmann-Rohrer, U.; Santoro, R.; Langst, G.; Grummt, I. NoRC—a novel member of mammalian ISWI-containing chromatin remodeling machines. *EMBO J.* **2001**, *20*, 4892–4900.
- (4) Zhou, Y.; Grummt, I. The PHD finger/bromodomain of NoRC interacts with acetylated histone H4K16 and is sufficient for rDNA silencing. *Curr. Biol.* **2005**, *15*, 1434–1438.
- (5) Gu, L.; Frommel, S. C.; Oakes, C. C.; Simon, R.; Grupp, K.; Gerig, C. Y.; Bär, D.; Robinson, M. D.; Baer, C.; Weiss, M.; et al. BAZ2A (TIP5) is involved in epigenetic alterations in prostate cancer and its overexpression predicts disease recurrence. *Nat. Genet.* **2015**, *47*, 22–30.
- (6) Peña-Hernández, R.; Aprigliano, R.; Carina Frommel, S.; Pietrzak, K.; Steiger, S.; Roganowicz, M.; Lerra, L.; Bizzarro, J.; Santoro, R. BAZ2A-mediated repression via H3K14ac-marked enhancers promotes prostate cancer stem cells. *EMBO Rep.* **2021**, *22*, No. e53014.
- (7) Bevil, S. M.; Olivares-Quintero, J. F.; Sciaky, N.; Golitz, B. T.; Singh, D.; Beltran, A. S.; Rashid, N. U.; Stuhlmiller, T. J.; Hale, A.; Moorman, N. J.; Santos, C. M.; Angus, S. P.; Zawistowski, J. S.; Johnson, G. L. GSK2801, a BAZ2/BRD9 Bromodomain Inhibitor, Synergizes with BET Inhibitors to Induce Apoptosis in Triple-Negative Breast Cancer. *Mol. Cancer Res.* **2019**, *17*, 1503–1518.
- (8) Spiliotopoulos, D.; Wamhoff, E. C.; Lolli, G.; Rademacher, C.; Caffisch, A. Discovery of BAZ2A bromodomain ligands. *Eur. J. Med. Chem.* **2017**, *139*, 564–572.

(9) Chen, P.; Chaikuad, A.; Bamborough, P.; Bantscheff, M.; Bountra, C.; Chung, C. W.; Fedorov, O.; Grandi, P.; Jung, D.; Lesniak, R.; Lindon, M.; Müller, S.; Philpott, M.; Prinjha, R.; Rogers, C.; Selenski, C.; Tallant, C.; Werner, T.; Willson, T. M.; Knapp, S.; Drewry, D. H. Discovery and Characterization of GSK2801, a Selective Chemical Probe for the Bromodomains BAZ2A and BAZ2B. *J. Med. Chem.* **2016**, *59*, 1410–1424.

(10) Drouin, L.; McGrath, S.; Vidler, L. R.; Chaikuad, A.; Monteiro, O.; Tallant, C.; Philpott, M.; Rogers, C.; Fedorov, O.; Liu, M.; Akhtar, W.; Hayes, A.; Raynaud, F.; Müller, S.; Knapp, S.; Hoelder, S. Structure enabled design of BAZ2-ICR, a chemical probe targeting the bromodomains of BAZ2A and BAZ2B. *J. Med. Chem.* **2015**, *58*, 2553–2559.

(11) Dalle Vedove, A.; Spiliotopoulos, D.; D'Agostino, V. G.; Marchand, J. R.; Unzue, A.; Nevado, C.; Lolli, G.; Caffisch, A. Structural Analysis of Small-Molecule Binding to the BAZ2A and BAZ2B Bromodomains. *ChemMedChem*. **2018**, *13*, 1479–1487.

(12) Sunseri, J.; Koes, D. R. Pharmit: interactive exploration of chemical space. *Nucleic Acids Res.* **2016**, *44*, W442–448.

(13) Sterling, T.; Irwin, J. J. ZINC 15–Ligand Discovery for Everyone. *J. Chem. Inf. Model.* **2015**, *55*, 2324–2337.

(14) Majeux, N.; Scarsi, M.; Apostolakis, J.; Ehrhardt, C.; Caffisch, A. Exhaustive docking of molecular fragments with electrostatic solvation. *Proteins* **1999**, *37*, 88–105.

(15) Goossens, K.; Wroblowski, B.; Langini, C.; van Vlijmen, H.; Caffisch, A.; De Winter, H. Assessment of the Fragment Docking Program SEED. *J. Chem. Inf. Model.* **2020**, *60*, 4881–4893.

(16) Marshall, M. S.; Steele, R. P.; Thanthirawatte, K. S.; Sherrill, C. D. Potential energy curves for cation- π interactions: off-axis configurations are also attractive. *J. Phys. Chem. A* **2009**, *113*, 13628–13632.

(17) Dalle Vedove, A.; Cazzanelli, G.; Corsi, J.; Sedykh, M.; D'Agostino, V. G.; Caffisch, A.; Lolli, G. Identification of a BAZ2A bromodomain hit compound by fragment joining. *ACS Bio & Med. Chem. Au* **2021**, *1*, 5–10.

(18) Lolli, G.; Battistutta, R. Different orientations of low-molecular-weight fragments in the binding pocket of a BRD4 bromodomain. *Acta Crystallogr. D Biol. Crystallogr.* **2013**, *69*, 2161–2164.

(19) Navratilova, I.; Aristotelous, T.; Picaud, S.; Chaikuad, A.; Knapp, S.; Filappakopoulos, P.; Hopkins, A. L. Discovery of New Bromodomain Scaffolds by Biosensor Fragment Screening. *ACS Med. Chem. Lett.* **2016**, *7*, 1213–1218.

(20) Lucas, X.; Wohlwend, D.; Hügle, M.; Schmidtkunz, K.; Gerhardt, S.; Schüle, R.; Jung, M.; Einsle, O.; Günther, S. 4-Acyl pyrroles: mimicking acetylated lysines in histone code reading. *Angew. Chem., Int. Ed. Engl.* **2013**, *52*, 14055–14059.

(21) Hügle, M.; Regenass, P.; Warstat, R.; Hau, M.; Schmidtkunz, K.; Lucas, X.; Wohlwend, D.; Einsle, O.; Jung, M.; Breit, B.; Günther, S. 4-Acyl Pyrroles as Dual BET-BRD7/9 Bromodomain Inhibitors Address BET α Insensitive Human Cancer Cell Lines. *J. Med. Chem.* **2020**, *63*, 15603–15620.

(22) Schäker-Hübner, L.; Warstat, R.; Ahlert, H.; Mishra, P.; Kraft, F. B.; Schliehe-Diecks, J.; Schöler, A.; Borkhardt, A.; Breit, B.; Bhatia, S.; Hügle, M.; Günther, S.; Hansen, F. K. 4-Acyl Pyrrole Capped HDAC Inhibitors: A New Scaffold for Hybrid Inhibitors of BET Proteins and Histone Deacetylases as Antileukemia Drug Leads. *J. Med. Chem.* **2021**, *64*, 14620–14646.

(23) Marchand, J. R.; Dalle Vedove, A.; Lolli, G.; Caffisch, A. Discovery of Inhibitors of Four Bromodomains by Fragment-Anchored Ligand Docking. *J. Chem. Inf. Model.* **2017**, *57*, 2584–2597.

(24) Marchand, J. R.; Lolli, G.; Caffisch, A. Derivatives of 3-Amino-2-methylpyridine as BAZ2B Bromodomain Ligands: In Silico Discovery and in Crystallo Validation. *J. Med. Chem.* **2016**, *59*, 9919–9927.

(25) Filappakopoulos, P.; Qi, J.; Picaud, S.; Shen, Y.; Smith, W. B.; Fedorov, O.; Morse, E. M.; Keates, T.; Hickman, T. T.; Felletar, I.; Philpott, M.; Munro, S.; McKeown, M. R.; Wang, Y.; Christie, A. L.; West, N.; Cameron, M. J.; Schwartz, B.; Heightman, T. D.; La Thangue, N.; French, C. A.; Wiest, O.; Kung, A. L.; Knapp, S.;

Bradner, J. E. Selective inhibition of BET bromodomains. *Nature* **2010**, *468*, 1067–1073.

(26) Clark, P. G.; Vieira, L. C.; Tallant, C.; Fedorov, O.; Singleton, D. C.; Rogers, C. M.; Monteiro, O. P.; Bennett, J. M.; Baronio, R.; Müller, S.; Daniels, D. L.; Méndez, J.; Knapp, S.; Brennan, P. E.; Dixon, D. J. LP99: Discovery and Synthesis of the First Selective BRD7/9 Bromodomain Inhibitor. *Angew. Chem., Int. Ed. Engl.* **2015**, *54*, 6217–6221.

(27) Humphreys, P. G.; Bamborough, P.; Chung, C. W.; Craggs, P. D.; Gordon, L.; Grandi, P.; Hayhow, T. G.; Hussain, J.; Jones, K. L.; Lindon, M.; Michon, A. M.; Renaux, J. F.; Suckling, C. J.; Tough, D. F.; Prinjha, R. K. Discovery of a Potent, Cell Penetrant, and Selective p300/CBP-Associated Factor (PCAF)/General Control Nonderepressible 5 (GCN5) Bromodomain Chemical Probe. *J. Med. Chem.* **2017**, *60*, 695–709.

(28) Wilson, J. E.; Patel, G.; Patel, C.; Brucelle, F.; Huhn, A.; Gardberg, A. S.; Poy, F.; Cantone, N.; Bommi-Reddy, A.; Sims, R. J., 3rd; Cummings, R. T.; Levell, J. R. Discovery of CPI-1612: A Potent, Selective, and Orally Bioavailable EP300/CBP Histone Acetyltransferase Inhibitor. *ACS Med. Chem. Lett.* **2020**, *11*, 1324–1329.

Recommended by ACS

Bivalent BET Bromodomain Inhibitors Confer Increased Potency and Selectivity for BRDT via Protein Conformational Plasticity

Xianghong Guan, Ernst Schönbrunn, *et al.*

JULY 22, 2022
JOURNAL OF MEDICINAL CHEMISTRY

READ 

Virtual Screening in the Cloud Identifies Potent and Selective ROS1 Kinase Inhibitors

Dušan Petrović, Jens Sadowski, *et al.*

AUGUST 03, 2022
JOURNAL OF CHEMICAL INFORMATION AND MODELING

READ 

GNE-064: A Potent, Selective, and Orally Bioavailable Chemical Probe for the Bromodomains of SMARCA2 and SMARCA4 and the Fifth Bromodomain of PBRM1

Alexander M. Taylor, Andrea G. Cochran, *et al.*

AUGUST 05, 2022
JOURNAL OF MEDICINAL CHEMISTRY

READ 

Discovery and Biological Characterization of PRMT5:MEP50 Protein–Protein Interaction Inhibitors

Andrew M. Asberry, Chang-Deng Hu, *et al.*

OCTOBER 07, 2022
JOURNAL OF MEDICINAL CHEMISTRY

READ 

Get More Suggestions >